RSC Advances

RSC Advances

www.rsc.org/advances

ROYAL SOCIETY
OF CHEMISTRY

www.rsc.org/advances

Journal Name

ARTICLE

Synthesis of Hierarchically Meso-Macroporous TiO₂ Film Based on UV Light-induced In Situ Polymerization: Application to Dye-sensitized Solar Cells

Quan Jin[b] † , Zhiwen Li[a] † , Kaifeng Lin[a], Shuo Wang[b], Rongguo Xu[b] and Dan Wang[a,b]*

Hierarchically meso-macroporous TiO₂ films were prepared via a UV light-induced in situ polymerization of hybrid organic-inorganic films containing propoxylated glyceryltriacrylate monomers and titania precursors. These films were composed of some well-connected net-like frameworks with large open cavity (0.2−1.5 μm), which themselves assembled by some titania nanocrystals with size of ~25 nm and possessed relatively rich inner crystal mesopores about 4 nm. The particular net-like frameworks make it a promising candidate for use as the scattering layer in dye-sensitized solar cells (DSSCs). The bilayer structured photo-electrode, consisting of the net-like framework layer on top of the P25 film, was prepared and exhibited overall conversion efficiency. Interestingly the photovoltaic conversion efficiency (η) was improved to 6.95%, much higher than that of P25 single layer film (6.17%).

1 Introduction

Since the breakthrough work into Dye-sensitized solar cells (DSSCs) in 1991 it has drawn much attention in the past decades, various attempts have been made to improve the efficiency of DSSCs.[1-10] As the core component in the DSSCs, the structures and properties of photoanode directly affect the photoelectron conversion efficiency. Recently, various novel photoanode materials have been developed towards improving the utilization of photoelectron.[5-10]

Nanocrystalline TiO₂ has been the most widely used photoanode material for DSSCs due to its superior stability and efficient electron injection efficiency.[11] Such photoanode materials normally possess large surface areas to maximize dye absorption for light harvesting. Usually, TiO₂ thin films composed of small NPs (20~30 nm) have higher surface area, leading to enhancing the light-harvesting efficiency, unfortunately, decreasing the light scattering. In order to solve this problem adding a scattering layer as an effective way has been attracting much attention. [10, 12-16]Currently, scattering layers can be formed by following some ways. (1) Mixing TiO₂ particles with different size and the larger particles were used as scattering center.[17] (2) Using polystyrene spheres as a template to form a film and then removed the polystyrene spheres to produce spherical voids that acted as scattering layer in the electrode.[18, 19] (3) TiO₂ nanorods and TiO₂ microplates could be used as scattering layer as well.[20-22] As we all know, the introduction of large particles would reduce the dye-loading capacity of the electrode. Therefore, a film-type scattering layer is more favorable for light harvesting.

As a result, more efforts have been devoted to prepare porous TiO₂ film with large surface area. Highly organized and oriented mesoporous TiO₂ thin films with various mesostructures, such as p6m, or Ia3d, Im3m have already been prepared.[23-25] Two groups of Grätzel and Li have investigated the mesoporous TiO₂ films exhibiting greatly enhanced performance in dye-sensitized solar cells, but the performance of actual cells is limited by incomplete filling of mesopores due to the smaller pore size (<10 nm),[26,27] and the existing preparation methods were so complex, not suitable for large scale production.

UV-curing is a facile way to prepare polymeric film from photosensitive monomers and the properties of synthesized film can be easily controlled by using different photosensitive monomer and irradiation condition.[28] In the present work, hierarchically mesoporous TiO₂ films with controllable hierarchical structure and properties was fabricated through UV light-induced in situ polymerization of hybrid organic-inorganic films containing photosensitive monomers and titania precursors with net-like frameworks. The as-prepared net-like frameworks (NF) film was further used as the scattering layer to construct a novel double layer (DL) film with the NF layer on top of the P25 layer. The introduction of NF layer increased the capacity of scattering light owing to its network structure with the branches around 300-500 nm. As a result, the photovoltaic conversion efficiency (η) was improved to 6.95%, much higher than that of P25 single layer film (6.17%). With FTO without NF layer, only a small fraction of the light is reflected and most of the solar energy is transmitted out of the system. Hence, due to the enhanced light scattering by the NF

layer, more electrons can be excited and then the photocurrent and photoelectrical conversion efficiency are increased.

2 Experimental Section

2.1 Materials

Titanium tetrabutoxide (TTB), anhydrous ethanol, N, N-dimethylformamide (DMF), polyvinylpyrroli-done (PVP, molecular weight ~ 30000), were all purchased from Beijing Chemical Reagents Co. Ltd. Propoxylatedglyceryltriacrylate (POGTA) was purchased from Tianjin Tianjiao Chemical Co. Ltd. 2, 2-dimethoxy-2-phenylacetophenone (Irgacure651) as photoinitiator, was purchased from Jingjiang Hongtai Chemical Engineering Co. Ltd. All the chemicals were used without further purification.

2.2 Preparation of Initial Precursor Solutions

A typical precursor solution was synthesized as follows: TTB was dissolved in the mixture of ethanol and DMF, stirred for 10 min. Then, the mixture of nitric acid and water was added under the ice/water cooled condition, in order to hydrolyze the inorganic precursor slowly. After taking off the cooled ice/water condition, POGTA, Irgacure 651 (1wt% of POGTA), and PVP (2wt% of the whole above sol) were slowly added, and stirred until fully dissolved, respectively. The molar ratio of TTB, ethanol, DMF, HNO_3, H_2O and POGTA was 1:8:4:0.5:3:0.9.

2.3 Preparation of Bilayer Film

The bilayer structured composite electrode was prepared as follows. To obtain the composite electrode, degussa P25 (25 nm-sized TiO_2 nanoparticles) was firstly coated over the fluorine-doped tin oxide (FTO) substrate by the doctor blade technique. Then TiO_2 films with net-like framework were deposited by dip-coating P25/FTO substrate at constant withdrawal rate of 2cm . min^{-1}. Immediately, the as-obtained fresh films were cured by UV light (generated by 16W low pressure mercury lamp, λ_{max} =253.7 nm, the distance of films and lamp is about 5 cm) for 5 min, and the resultant gel films were calcined at 200 ^{o}C for 20 min and then at 500 ^{o}C for 60 min. The whole procedure is displayed in Scheme 1.
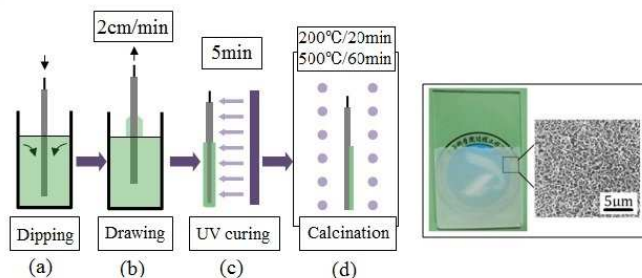
Scheme 1. The preparing procedure of porous TiO_2 film with net-like frameworks: (a) Dipping in the precursor solutions for TiO_2 coatings. (b) Withdrawal step with a lifting speed 2 cmmin^{-1}. (c) UV curing step and formation of the gel film on the glass slide. (d) Calcinations step for the forming of the porous TiO_2 film with net-like frameworks with treating the gel film at 200°C for 20 min and then at 500 ^{o}C for 60 min. (e) Porous TiO_2 film obtained by dip-coating from precursor solutions.

2.4 Characterization

SEM images were obtained using a JEOL JSM-6700F scanning electron microscope at 3.0 kV. UV-vis spectrophotometry was carried out with UNICO UV-2802PC. Nitrogen adsorption-desorption isotherms were collected using Quantachrome Instruments Autosorb-1 equipment on samples scratched off as-prepared films. The *I-V* characteristics of the cell were measured by an electrochemical analyzer (CHI630A, Chenhua Instruments Co., Shanghai) under solar simulator illumination (CMH-250, Aodite Photoelectronic Technology Ltd., Beijing) at room temperature. The monochromatic incident photon-to-electron conversion efficiency (IPCE) was measured by illumination with monochromatic light, which was obtained by a series of light filters with different wavelengths. The EIS was carried out on a Zahner IM6e impedance analyzer (Germany) in the frequency range of 0.02 Hz to 100 kHz with illumination of 100 mW/cm^2.

2.5 Photocatalysis Test

The photocatalytic activity of TiO_2 films was tested for the degradation of methylene blue (MB) in aqueous solution. An 18 W UV fluorescent bulb with 365 nm was used as the light source. In each run, TiO_2 film (all samples were cut into squares with same sizes of about 7.0 mm × 25.6 mm) was added into 2 mL of MB solution (2 × 10^{-5} M). Prior to photocatalytic reaction, the system was kept in dark, and the concentration of MB was monitored. The concentration of MB did not change after 60 min, which indicates that it is enough to reach the adsorption equilibrium of MB for 60 min. The MB concentration was determined by measuring the maximum absorbance around λ = 664 nm in UV-vis absorption spectra.

3 Results and discussion

3.1 The morphology and structure of films
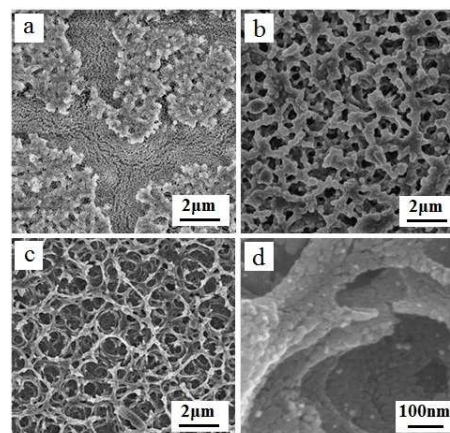

Figure 1. SEM images of (a) non-UV cured gel film. (b) UV cured gel film. (c) Porous TiO_2 film obtained after calcination. (d) High magnification image of film in the (c).

The morphology evolution of the films was shown in Figure 1. The non-UV irradiated gel film obtained via dip-coating method had many cracks in the film (Figure 1a). However, after UV irradiation some net-like frameworks of hybrid polymer-titania composite with large open cavity (0.2−1.5 μm) could be observed in the gel film (Figure 1b). Further by calcinations, porous TiO_2 film with anatase phase was obtained (XRD pattern see figure S1 in supporting information). The as-

prepared porous TiO_2 film shows well-connected net-like framework, forming three dimensional porous structures (Figure 1c). Compared to the porous gel film, the net-like framework becomes slender, changed from 600 nm to 150 nm, which may be attributed to getting rid of organic parts and the shrinkage of inorganic parts during the heat-treatment process. From the high magnification SEM image of TiO_2 film (Figure 1d), it is obvious that the net-like framework of TiO_2 film is composed of nanoparticles around 25 nm, and there is fruitful porous structure formed by the net-like frameworks with pores opening between 200 nm to 1.5 μm. This was also supported by TEM and HRTEM images of the film (see Figure S2 in supporting information). To determine the specific surface area of the NF film, Brunauer-Emmett-Teller (BET) nitrogen absorption/desorption analysis is performed. The BET surface area is 46 m^2g^{-1} and total porous volume is 0.14 cm^3g^{-1}. The materials present the typical type IV N_2 sorption isotherms with a H3 hysteresis loop, which is usually considered to be indicative of gas adsorption in the mesopores.[29] The pore size was 3.8 nm. (See Figure S3 in supporting information).

3.2 FTIR analysis of UV-cured gel film

Figure 2 shows the FT-IR spectra of POGTA monomer including the unirradiated gel film and the irradiated gel film. Some peaks appeared at 1638 cm^{-1} and 1620 cm^{-1}, which are assigned to C=C stretching of acrylates in the POGTA monomer.[30] These peaks are observed distinctly in the spectra of the unirradiated gel film, despite the disturbance from a wide strong peak around 1650 cm^{-1} attributed to C=O stretching of PVP [31] (Figure 2b), while they are undistinguishable in that of the irradiated gel film. Moreover, the peaks of other groups in POGTA could be easily identified in the spectra of both unirradiated and irradiated gel film. All of the above results indicate that the monomers in the film were polymerized even under UV irradiation for short time, which has been also argued in other reports.[30,32]
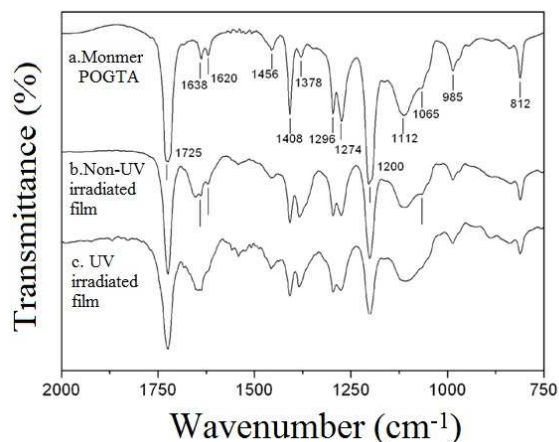

Figure 2. FTIR spectra of (a) Monomer POGTA. (b) The non-UV irradiated gel film. (c) The UV irradiated gel film.

3.3 The influences of precursor prescription

The prepared composite film showed a good DL structure. However, the NF layer structure was highly affected by the initial precursor solution and then further influenced the light scattering and photoelectric conversion efficiency.

Accordingly, a detailed investigation of the influences of precursor prescription was taken from theory and experiment.

In the initial precursor solution, the originating hydrolysis and condensation of TTB was hardly to be occurred because of the highly acidic circumstance and low water content condition. It could be proposed that only small oligomeric Ti-oxo clusters were mainly formed. PVP is an amphiphilic polymer which can be interacted with the Ti-oxo clusters by hydrogen bond, forming a composite Ti-oxo-PVP,[33] as shown in Scheme 2a. In UV irradiation process, radicals can be produced not only on photosensitive monomer POGTA, but also on macromolecular PVP chains. If the molar ratio between POGTA and PVP is suitable, the organic monomer will be surrounded by the macromolecular chains of PVP. As a result, the UV-induced photo-graft-polymerization of POGTA and PVP becomes the dominated reaction approach,[34,35] as shown in Scheme 2b. If the above two interactions take place at same time, the fresh dip-coated film is no longer homogeneous in the UV curing process. Moreover, the composites of Ti-oxo-PVP congregates, which is motivated by the graft-polymerization of POGTA to PVP. During the congregating process, a network may be fabricated. On the other hand, due to the evaporation of the solvent in the fresh film, the inorganic polymerization will be accelerated and then solidify the network subsequently. The local place where is absence of Ti-oxo-PVP composites, forms cavities after the evaporation of the solvent. Finally, porous gel film was prepared by the UV-curing process. Further by appropriate calcinations, the porous structure is maintained, and porous TiO_2 film is synthesized.
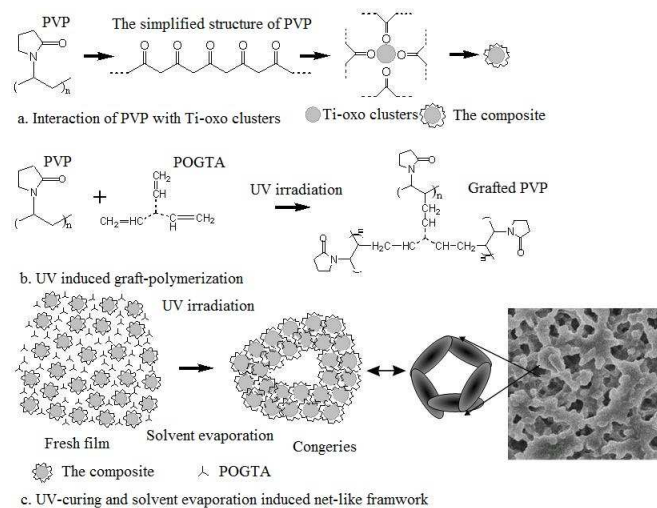
Scheme 2. The possible mechanism of the synthesized porous TiO_2 film with net-like framework by UV-curing method.

A detailed experimental study was conducted about the precursor solutions. The molar ratio of solvent (EtOH/DMF=2, 1 and 0.5) was changed based on the typical composition of the precursor sol, different morphologies of TiO_2 films, i.e., TF-0, TF-1 and TF-2, were prepared, whose SEM images are shown in Figure 3. Along with the increasing of the molar ratio of DMF, the apparent porosity of the as-prepared TiO_2 films decreases clearly. TF-0 is porous film with net-like framework, just as shown in Figure 1d. TF-1 preserves the net-like framework but with larger size. For TF-2, the morphology of net-like framework is disappeared and replaced by sparse round holes. And Figure 3d indicates that TF-2 is composed of TiO_2 nanoparticles. It is obvious that the apparent porosity of the as-

prepared TiO_2 films was sharply decreased as the molar ratio of DMF increasing. In order to understanding the above phenomenon, the thermal dynamic property of binary mixed solution EtOH-DMF was investigated. It was found that excess functions of the solution, such as excess intermolecular free length and excess free energy, achieved minima when the molar fraction of DMF is 0.35, indicating the strong interaction between DMF and ethanol molecules, leading to the formation of a DMF-ethanol complex.[36] Therefore, the volatility and saturated vapor pressure of the mixed solution is minimum as the molar ratio of solvent EtOH/DMF=2 ($x_{DMF} \approx 0.35$), making the fresh dip-coated film maintain wet for the longest time. Moreover, the wetness of the fresh film benefits UV-induced polymerization of monomers, and motivated matter transfer in the fresh film, which is the right reason for the preparation of porous TiO_2 film. Consequently, as EtOH/DMF=2, the prepared TiO_2 film, TF-0, exhibits the highest porosity, and as increasing DMF molar ratio, the apparent porosity of the as-prepared TiO_2 films reduces.
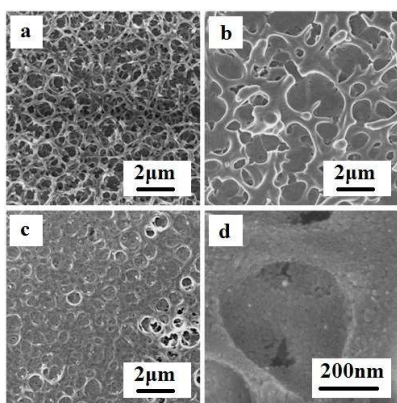

Figure 3. SEM images of (a)TF-0. (b)TF-1 and (c)TF-2 films when the molar ratio of solvent EtOH/DMF=2, 1 and 0.5, respectively, and high magnification of TF-2(d).

Changing the molar ratio of nitric acid (HNO_3/TTB = 0.3, 0.5, 0.7 and 0.8) based on the typical composition of the precursor sol, different morphologies of TiO_2 films, i.e. TF-3, TF-0, TF-4 andTF-5, were prepared, whose SEM images are shown in Figure 4. Considering that inorganic polymerization can be readily controlled by the acidity of precursor sol, when the inorganic polymerization rate is restrained to equivalent to the UV-induced organic polymerization rate, it is efficiently to utilize the structure directing agent in situ synthesized. The molar ratio (HNO_3/TTB = 0.5) may be the optimum. Porous film TF-0 with net-like framework was fabricated. Reducing the acidity to HNO_3/TTB = 0.3, the indiscriminate condensation of inorganic precursor takes place, hindering template effect of organic polymer synthesized in UV irradiation process. Ultimately, film TF-3 only with sparse holes was prepared. Improving acidity to HNO_3/TTB = 0.7, the UV-induced organic polymerization rate is relatively higher, making the size of fabricated net-like framework in TF-4 relatively larger. However, when the acidity increased to HNO_3/TTB = 0.8, possibly due to high density of inorganic colloid, the interaction between the inorganic colloid and the structure directing agent is weakened. Therefore, the morphology of net-like framework is disappeared, replaced as nearly dense film TF-5 was prepared. And the big magnification SEM images of the as-prepared TiO_2 films indicate that all the films are composed of TiO_2 nanoparticles.

Changing the amount of PVP (0wt%, 1wt%, 2wt%, 4wt%, 5wt% and 6wt%) based on the typical composition of the precursor sol, different morphologies of TiO_2 films, i.e. TF-6, TF-7, TF-0, TF-8, TF-9 and TF-10, were prepared, whose SEM images are shown in Figure 5. Apparently, when no PVP was added, only small islands grew on dense film. When the amount of PVP added up to 1wt%, the small islands were connected each other to form arborization structure. Increasing PVP addition to 2wt%, net-like framework was fabricated. Increased to 4wt%, some cracks has been appeared, together with net-like framework. However, when PVP addition achieved 5wt%, net-like framework in the whole region of the film began to disappear, while a lot of locals featured with net-like framework still exited. When the PVP addition increased to 6wt%, the net-like framework disappeared completely, resulting in a nearly dense film. Therefore, the PVP addition is an key parameters controlling from the formation of net-like framework to vanish.
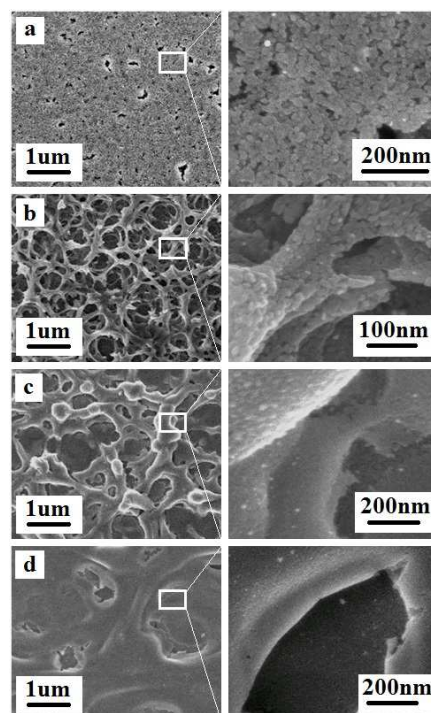
Figure 4. SEM images of (a)TF-3, (b)TF-0, (c)TF-4 and (d)TF-5 films when the molar ratio HNO_3/TTB =0.3, 0.5, 0.7 and 0.8, respectively.
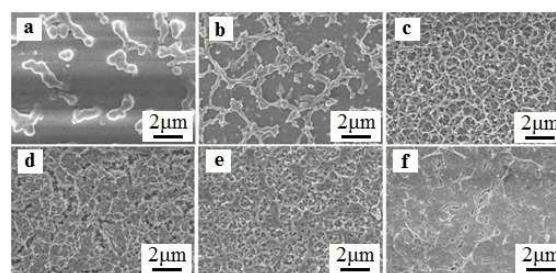
Figure 5. SEM images of (a)TF-6, (b)TF-7, (c)TF-0, (d)TF-8, (e)TF-9 and (f)TF-10 films when PVP added 0wt%, 1wt%, 2wt%, 4wt%, 5wt% and 6wt%, respectively.

Changing the molar ratio of organic monomer (POGTA/TTB =0.3, 0.6, 0.9, 1.0 and 1.1) based on the typical composition of

the precursor sol, different morphologies of TiO_2 films, i.e. TF-11, TF-0, TF-12, TF-13 and TF-14, were prepared, whose SEM images are shown in Figure 6. UV-induced organic monomer polymerization is the real reason for the preparation of porous TiO_2 film. Therefore, when no organic monomer was added, only dense film composed of nanoparticles was synthesized (see supporting information Figure S4). POGTA/TTB = 0.9 may be the optimized molar ratio. Possibly due to appropriate size of structure directing agent formed in the UV irradiation process, porous film with biggest apparent porosity and fruitful of net-like framework was prepared. Reducing monomer amount, none of net-like framework was formed and the porosity of prepared films (TF-11 and TF-0) decreased. However, improving the amount of monomer to POGTA/TTB =1.0 and 1.1, as more enough template synthesized, the porosity of film TF-13 and TF-14 was also decreased compared to TF-12. The obtained DL-films with different NF layer morphology, i.e.,DL-TF-11, DL-TF-0, DL-TF-12, DL-TF-13 and DL-TF-14, were used as the composite electrode to investigate their photo catalytic properties.
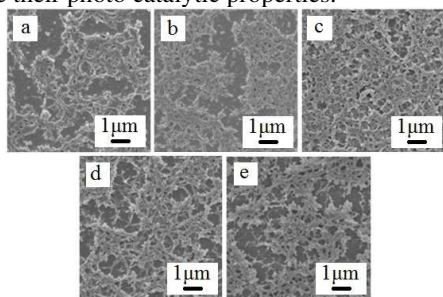
Figure 6. SEM images of: (a)TF-11, (b)TF-0, (c)TF-12, (d)TF-13 and (e)TF-14 films when the molar ratio POGTA/TTB = 0.3, 0.6, 0.9, 1.0 and 1.1, respectively.

3.4 Photovoltaic behavior of DSSCs

As shown in Figure 7a, the TiO_2 films with net-like framework were used as the scattering layer to form a novel DL-film which was used as the photoanode of DSSCs. The overlayer seems firmly attached on the P25 layer, whose thickness is about 3 μm (Figure 7b). The photocatalytic properties of the prepared photoanode were summarized in Table 1. The sample DL-TF-12 was found to display the best photovoltaic performance with short-circuit photocurrent density (J_{sc}) of 14.28 mAcm^{-2}, open-circuit voltage (V_{oc}) of 0.68 V, and conversion efficiency (η) of 6.57%. However, the BET surface area of 35.7 $m^2 g^{-1}$ for this sample with the lowest value among all the samples. The improving of the photoelectron utilization is attributed to the network layer with plentiful branches of the material which can effectively improve the light scattering. Hence, more solar energy is constrained in the solar cells, increasing light intensity and improving the photocurrent. The DL-TF-12 network layer was used for the following research, and the thickness of the network layer was 3 μm.
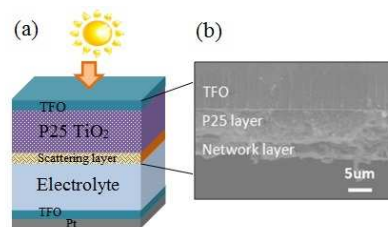
Figure 7 (a) Schematic diagram of the dye sensitized solar cell: the photoanode was prepared by a novel bilayer structured film which use the TiO_2 films with net-like framework as the scattering layer on top of the P25 layer. (b) the cross section SEM image of the as- prepared bilayer-structure film.

The effect of the thickness of P25 layer was also investigated. The photovoltaic performance of DL-films with different thickness of P25 layer (7 μm, 8 μm, 9 μm and 10 μm), i.e. DL-P-7, DL-P-8, DL-P-9 and DL-P-10 were summarized in Table 2, and pure P25 single layer film (SL-film) was test as contrast. The cells derived from all the DL-films demonstrate considerably improved conversion efficiency (η) compared to that of the SL-film. With increasing the thickness of P25 layer of DL-films conversion efficiency was firstly increased then decreased, and P25 layer with the thickness of 8 μm shown the best conversion efficiency (6.95%) which increased by 12.6% compared to the SL-film. However, the saturated dye adsorption capacity of DL-film (1.27×10^{-7}mol cm^{-2}) was lower than that of P25 (1.36×10^{-7}mol cm^{-2}), the dye adsorption capacity is reduced by seven percent which may be attributable to the considerably lower surface areas of the DL-film. It means the DL-film has a higher utilization of the adsorbed photoelectron. Accompanied by the branches of the network layer, light scattering was enhanced and cell performance was improved as well. This can be proved by further optical measurements. Sample DL-P-8 was used to compare with only P25 layer owing to its outstanding photovoltaic performance.

Table 1. Photovoltaic properties of the DSSCs composed of bilayer film photo electrode with different net-work layer [a].

Electrode [b]	V_{oc}(V)	I_{sc} (mA/cm^2)	FF (%)	η (%)
DL-TF-11	0.67	13.21	70.84	6.27
DL-TF-0	0.67	13.92	68.09	6.35
DL-TF-12	0.68	14.28	67.66	6.57
DL-TF-13	0.67	13.52	71.20	6.45
DL-TF-14	0.67	13.22	71.35	6.32

[a] Photovoltaic parameters of different electrodes. Measure condition: simulate sunlight (AM1.5, 100 mWcm^{-2}). The sensitizer was N_3 (ruthenium dye). The cell active area was 0.20 cm^2, and the light intensity was 100mWcm^{-2}. The values shown are from cells, based on averages of about ten samples.
[b] The P25 layer and network layer thickness were 10 um and 3 um, respectively.

Table 2. Photovoltaic properties of the DSSCs composed of bilayer photo electrode with different thickness of the P25 layer [a].

Electrode[b]	Voc(V)	Isc(mA/cm^2)	FF(%)	η(%)
SL- P25	0.69	15.58	57.39	6.17
DL-P-7	0.71	16.41	59.05	6.88
DL-P-8	0.69	17.07	59.01	6.95
DL-P-9	0.69	16.06	59.83	6.63
DL-P-10	0.68	14.18	68.24	6.58

[a] Photovoltaic parameters of different electrodes. Measure condition: simulate sunlight (AM1.5, 100mWcm^{-2}). The sensitizer was N_3 (ruthenium dye). The cell active area was 0.20 cm^2, and the light intensity was 100 mWcm^{-2}. The values shown are from cells, based on averages of about ten samples. [b] The net-work layer was prepared by POGTA/TTB=0.9, and the thickness was 3 μm.

3.5 UV-Vis

The reflectivity of each film with and without dye loading was studied to investigate the scattering efficiency of the DL-film and SL-film P25, Figure 8a. Compared to SL-film electrode, DL-film with network layer brings an increasing reflectance over the entire wavelength range. Before the dye adsorption, both DL-film and SL-film had high reflectivity. However, the reflectivity of P25 film became lower than that of DL-film in the wavelength range over 500 nm, indicating the network layer of the DL-film had a better light-scattering ability than those in the SL-film due to the comparable branches of network layer to the wavelength of visible light. After dye adsorption, the incident light was absorbed by the dye molecules, the reflectance of the DL-film decreased drastically to ca.33% in the short wavelength ranging from 400 to 550 nm (Figure 8b). However the dye-absorbed DL-film remained a substantially higher reflectance than the dye-absorbed P25 film in the wavelength region over 450 nm which further supports our argument about the better light scattering property of the network layer structure result in higher conversion efficiency of the DL-film compared to P25 SL-film.

(A)

(B)
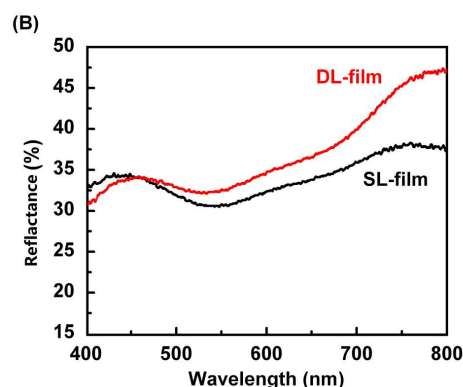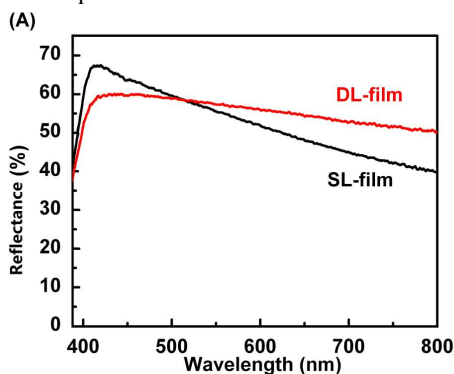
Figure 8. Diffused reflection patterns of the single layer film (SL-film: only P25 layer) and double layer film (DL-film: TiO$_2$ films with net-like framework on top of the P25 layer, sample DL-P-8) (A) before dye absorbed; (B) after dye absorbed.

3.6 Incident photon-to-current conversion efficiency (IPCE) performance

The IPCE spectra for the DSSC cells provide further evidence on the scattering effect of the bilayer structures (Figure 9). Compared to SL-film, the IPCE response over the entire range of light was enhanced. The peak value of the IPCE was increased by 30% for IPCE$_{630}$ with DL-film electrode. The enhanced IPCE provides more evidence of the superior optical characteristic of the bilayer structures of DL-film. The DL-film electrode showed a higher incident photon-to-current conversion efficiency. An enhancement in light conversion efficiency from 580 nm until far in the absorption tail (up to 750 nm) can be observed, which may be attributed to the superior light scattering properties of network layer on top of the DL-film, especially in the long wavelength region. This result highly consists with the UV-vis diffuse reflectance spectrum.
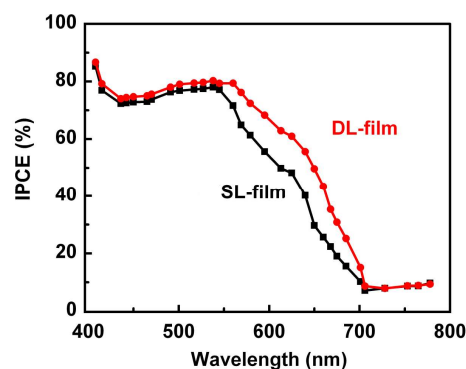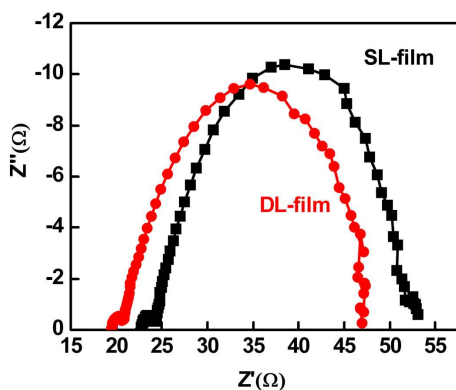

Figure 9. The normalized IPCE spectra of DSSCs based on single layer film (SL-film: only P25 layer) and double layer film (DL-film: TiO$_2$ films with net-like framework on top of the P25 layer, sample DL-P-8).

3.7 Electrochemical Impedance Spectra (EIS) Measurement of Different Electrodes

EIS is a useful method to clarify the electronic and ionic transport processes in DSSCs. To further confirm the effect of network layer in enhancing the light scattering in the DSSCs, the SL-film and DL-film were characterized by EIS which was

measured under the illumination of one sun at open-circuit potential. As shown in Figure 10, the Nyquist plots consist of two semicircles. The biggest semicircle at medium frequencies is attributed to photo injected electrons in the TiO_2 or back reaction from the injected electrons in TiO_2 to the electrolyte, which is the most important in the device. As shown, the semi-cycle at intermediate frequency region was decreased for electrode DL-film, indicating the fast redox activity of the electrolyte in the working electrode interface.

Figure 10. Nyquist of the electrochemical impedance spectra of electrodes prepared by single layer film (SL-film: only P25 layer) and double layer film (DL-film: TiO_2 films with net-like framework on top of the P25 layer, sample DL-P-8).

4 Conclusions

DL-film with the NF layer on top of the P25 layer are prepared and applied as photoanode of dye-sensitized solar cells (DSSCs). The NF layer with hierarchically meso-macroporous was prepared via a UV light-induced in situ polymerization of hybrid organic-inorganic films containing propoxylated glyceryltriacrylate monomers and titania precursors. A tentative mechanism was proposed to elucidate the preparation of porous TiO_2 film by UV induced in situ polymerization. The corresponding results of DSSCs made with DL-films are compared to that with SL-films. It is observed that DSSCs prepared with DL-films show higher conversion efficiency than those with SL-films. Furthermore, the highest efficiency (6.95%) is realized for DSSCs made using DL-film with 3 μm NF layer (prepared by POGTA/TTB=0.9) and 8 μm P25 layer. Nevertheless the saturated dye adsorption capacity of DL-film (1.27×10^{-7} mol cm^{-2}) was lower than that of P25 (1.36×10^{-7} mol cm^{-2}) which means the DL-film has a higher utilization of the adsorbed photoelectron. Accompanied by the branches of the network layer, light scattering was enhanced and improves cell performance.

Acknowledgements

Notes and references

[a] Academy of Fundamental Interdisciplinary Sciences, Harbin Institute of Technology, Harbin, Heilongjiang, P. R. China.
*E-mail:danwang@ipe.ac.cn
[b] State Key Laboratory of Multi-phase Complex System, Institute of Process Engineering, Chinese Academy of Sciences, 100190Beijing, P. R. China.
† These Authors contributed equally

1 B. O'regan and M. Grfitzeli, *Nature*, 1991, **353**, 737-740.
2 M. Grätzel, *Nature*, 2001, **414**, 338-344.
3 M. Yang, D. Kim, H. Jha, K. Lee, J. Paul and P. Schmuki, *Chem. Comm.*, 2011, **47**, 2032-2034.
4 P. M. Sommeling, B. C. O'regan, R. R. Haswell, H. J. P. Smit, N. J. Bakker, J. J. T. Smits and J. A. M. Van Roosmalen, 2006, *J. Phys. Chem .B,* **110**,19191-19197.
5 S. H. Ko, D. Lee, H. W. Kang, K. H. Nam, J. Y. Yeo, S. J. Hong and H. J. Sung, *Nano Lett.,* 2011, **11**, 666-671.
6 H. J. Koo, Y. J. Kim, Y. H. Lee, W. I. Lee, K. Kim and N. G. Park , *Adv. Mater.,* 2008, **20**, 195-199.
7 Y. Qiu, W. Chen and S. Yang, *Angew. Chem. Int .Ed.,* 2010, **122**, 3757-3761.
8 N. Yang, J. Zhai, D. Wang, Y. Chen and L. Jiang, *Acs Nano*, 2010, **4**, 887-894.
9 X. Wu, G. Q. M. Lu and L. Wang, *Energy Environ. Sci.*, 2011, **4**, 3565-3572.
10 N. Yang, Q. Yuan, J. Zhai, T. Wei, D. Wang and L. Jiang, *ChemSusChem.*, 2012, **5**, 572-576.
11 J. G. Nam, E. S. Lee, W. C. Jung, Y. J. Park, B. H. Sohn, S. C. Park, J. S. Kim and J. Y. Bae, *Mater. Chem. Phys.*, 2009, **116**, 46-51.
12 M. Zukalova, A. Zukal, L. Kavan, M. K. Nazeeruddin, P. Liska and M. Grätzel, *Nano Lett.*, 2005, **5**, 1789-1792.
13 K. Zhu, N. R. Neale, A. Miedaner and A. J. Frank, *Nano Lett.*, 2007, **7**, 69-74.
14 I. G. Yu, Y. J. Kim, H. J. Kim, C. Lee and W. I. Lee, *J. Mater. Chem.*, 2011, **21**, 532-538.
15 I. G. Yu, Y. J. Kim, H. J. Kim, C. Lee and W. I. Lee, J Mater. Chem., 2011, 21, 532-538.J. Y. Liao, B. X. Lei, D. B. Kuang and C. Y. Su, *Energy Environ. Sci.* , 2011, **4**, 4079-4085.
16 J. Y. Liao, B.X. Lei, H. Y. Chen, D. B. Kuang and C. Y. Su, *Energy Environ. Sci.,* 2012, **5**, 5750-5757.
17 Z. S. Wang, H. Kawauchi, T. Kashima and H. Arakawa, *Coord. Chem. Rev.*, 2004, **248**, 1381-1389.
18 J. Du, X. Lai, N. Yang, J. Zhai, D. Kisailus, F. Su, D. Wang and L. Jiang, *ACS Nano*, 2011, **5**, 590–596.
19 S. Hore, P. Nitz, C. Vetter, C. Prahl, M. Niggemann and R. Kern, *Chem. Comm.*, 2005, **15**, 2011-2013.
20 J.H. Yoon, S. R. Jang, R. Vittal, J. Lee and K. J. Kim, *J. Photoch. Photobio. A*, 2006, **180**, 184-188.
21 I. S. Cho, Z. Chen, A. J. Forman, D. R. Kim, P. M. Rao, T. F. Jaramillo and X. Zheng, *Nano letters*, 2011, **11**, 4978-4984.
22 W. Peng and L. Han, *J. Mater. Chem.*, 2012, **22**, 20773-20777.
23 D. Grosso, G. Soler-Illia, F. Babonneau, C. Sanchez, P. A. Albouy, A. Brunet-Bruneau and A. R. Balkenende, *Adv. Mater.,* 2001, **13**, 1085-1090.
24 E. L. Crepaldi, G. J. d. A. Soler-Illia, D. Grosso, F. Cagnol, F. Ribot and C. Sanchez, *J. Am. Chem. Soc.,* 2003, **125**, 9770-9786

25 W. Zhou and H. Fu, ChemCatChem., 2013, **5**, 885-894.

26 M. Zukalova, A. Zukal, L. Kavan, M. K. Nazeeruddin, P. Liska and M. Grˉatzel, *Nano Lett.*, 2005, **5**, 1789-1792.

27 K. Hou, B. Z. Tian, F. Y. Li, Z. Q. Bian, D. Y. Zhao and C.H. Huang, *J. Mater. Chem.*, 2005, **15**, 2414-2420.

28 C. Decker, L. Keller, K. Zahouily and S. Benfarhi, *Polymer*, 2005, **46**, 6640-6648.

29 J. Qi, J. Chen, G.D. Li, S.X. Li, Y. Gao and Z.Y. Tang, *Energy Environ. Sci.,* 2012, **5**, 8937–8941.

30 P. Yuan, H. He, F. Bergaya, D. Wu, Q. Zhou and J. Zhu, *Micro. Meso. Mater.*, 2006, **88**, 8-15.

31 V. Vijayabaskar, S. Bhattacharya, V. K. Tikku and A. K. Bhowmick, *Radiat. Phys. Chem.*, 2004, **71**, 1045-1058.

32 C. Leger, Q. T. Nguyen, J. Neel and C. Streicher, *Macromolecules*, 1995, **28**, 143-151.

33 A. Ali, A. K. Nain and M. Kamil, *Thermochimica acta*, 1996, **274**, 209-221.

34 J. M. Song, J. H. Zhu and S. H. Yu, *J. Phys. Chem. B.,* 2006, **110** , 23790-23795.

35 H. J. Chun, S. M. Cho, Y. M. Lee, H. K. Lee, T. S. Suh and K. S. Shinn, *J. Appl. Polym.*, 1999, **72**, 251-256.

36 P. S. Majumder and A. K. Bhowmick, *J. Appl. Polym. Sci.*, 2000, **77**, 323-337.

RSC Advances Accepted Accepted Manuscript